

# CFD Analysis of a Heat Collector Element in a Solar Parabolic Trough Collector

S. Mathew, G. Visavale\* & V. Mali

Centre for Computational Technologies, CFD Training Division,  
Shivajinagar, Pune, India 411 005.

Telephone: +91-9604 261 312, Email: [ganesh@cctech.co.in](mailto:ganesh@cctech.co.in)

## Abstract

A numerical study of the performance of a solar Parabolic Trough Collector (PTC) has been done focusing on its receiver. The receiver consisting of a glass-shield enclosing a Heat Collector Element (HCE) with vacuum in the annular space has been subjected to seasonal and diurnal variations of solar radiation along with the concentrated heat flux reflected from the parabolic trough mirror for conditions at Pune, India. The HCE is modeled as a metallic tube with thermic fluid Therminol-VP1™ flowing through it at low Reynolds number under thermally developing conditions with highly temperature dependent properties. The highly asymmetric nature of the physics for thermal and turbulent flow conditions make it imperative to consider a complete three dimensional domain for the conjugate heat transfer analysis. The conduction, convection and radiation heat transfer effects have been modeled with radiation restricted within the annular region using the S2S radiation model. The solar fluxes have been modeled using the Solar Load Model also accounting for the shadowing effects for semi-transparent and opaque surfaces. The pressure drop in the thermic fluid flow is comparatively uniform throughout the day during winter conditions while the fluid gets heated up 4 times more at noon compared to morning. The summer conditions exhibit a 2.5 times higher pressure drop at noon compared to the morning conditions. The comprehensive analysis is performed using the finite volume based CFD code of ANSYS FLUENT 12.1 and verifies the huge potential that PTC holds for high temperature applications in concentrated solar power plants.

Keywords: CFD, parabolic trough collector, S2S radiation model, heat collector element.

## 1. Introduction

Solar radiation is a high-temperature, high-exergy energy source at its origin, the Sun, where its irradiance is about  $63 \text{ MW/m}^2$ . However, Sun–Earth geometry dramatically decreases the solar energy flow down to around  $1 \text{ kW/m}^2$  on the Earth's surface. Nevertheless, under high solar flux, this disadvantage can be overcome by using concentrating solar systems which transform solar energy into another type of energy (usually thermal). Solar radiation is converted into thermal energy in the focus of solar thermal concentrating systems. These systems are classified by their focus geometry as either point-focus concentrators (central receiver systems and parabolic dishes) or line-focus concentrators (parabolic-trough collectors or PTCs) and linear Fresnel collectors. PTCs focus direct solar radiation onto a focal line on the collector axis. A receiver tube with a fluid flowing inside that absorbs concentrated solar energy from the tube walls and raises its enthalpy in this focal line. The collector is provided with one-axis solar tracking to ensure that the solar beam falls parallel to its axis<sup>[1]</sup>.

The applications of PTC can be divided into two main groups, the first and most important is Concentrated Solar Power (CSP) plants (with temperature requirements of  $300$  to  $400^\circ\text{C}$ ) and second being for the Industrial Process Heat (IPH) (with temperature requirements of  $100$  to  $250^\circ\text{C}$ ). The heat collector element (HCE) is a key component in parabolic trough solar thermal generation system, used to convert solar radiation to thermal energy. Optimizing its performance and improving its efficiency have important effects on the thermal-electricity conversion efficiency. The collector tube consists of inner metal absorber tube and the outer glass cover tube. The solar radiation is reflected to the outer surface of inner tube by parabolic trough and absorbed by tube wall, as is shown in Fig. 1. As a result, a majority of the energy will be conducted to the inner surface of inner tube and transferred by the working fluid in inner tube with mixed convective heat transfer.

In recent years, a lot of research has been performed for all kinds of solar receivers. While some aimed at cost reduction and performance improvements by new designs, others had been focused on improving the receiver tube reliability, selective coating performance, and new measurement methods for testing the parabolic trough system<sup>[2,3]</sup>. Most of the models on simulation studies with 1-D or 2-D analysis, always assumed that the solar flux and flow are uniform, and many correlations in the models are also based on a uniform temperature. However, because of the non-uniform solar flux on the outer surface of the inner absorber

tube, the flow will be heated asymmetrically and thus will be non-uniform. The present study focuses on analyzing the heat transfer phenomenon by comprehensively modeling the HCE using finite volume based CFD code of ANSYS FLUENT 12.1. The solar ray has been traced all throughout the day for a representative summer and winter day as being the summer solstice and the winter solstice at the location in Pune, India (Geographical location: N 17.5° to 19.2° & E 73.2° to 75.1°).

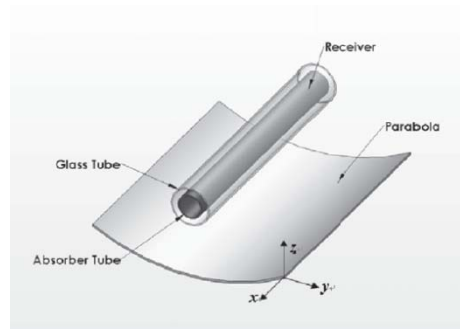


**Fig. 1** Schematic view of the Solar parabolic trough collector

## 2. Modeling the Heat Collector Element (HCE):

The assembly at the geometrical focus of the parabolic trough consists of a metallic tube enclosed within an evacuated cylindrical glass-shield. The metallic tube is the HCE within which the thermic fluid<sup>[4]</sup> Therminol-VP1™ is flowing. The fluid properties are highly temperature dependent and the required functions for these properties have been reported in the User Guide Manual, listed in Table 1.

**Table 1.** Properties of Therminol-VP1 as a function of temperature

Property	Equation (T in °C)
Density, (kg.m <sup>-3</sup> )	$0.90797 \times T(^{\circ}\text{C}) + 0.00078116 \times T2(^{\circ}\text{C}) - 2.367 \times 10^{-6} \times T3(^{\circ}\text{C}) + 1083.25$
Heat Capacity, (J.kg <sup>-1</sup> .K <sup>-1</sup> )	$0.002414 \times T(^{\circ}\text{C}) + 5.9591 \times 10^{-6} \times T2(^{\circ}\text{C}) - 2.9879 \times 10^{-8} \times T3(^{\circ}\text{C}) + 4.4172 \times 10^{-11} \times T4(^{\circ}\text{C}) + 1.498$
Thermal Conductivity, (W.m <sup>-1</sup> . K <sup>-1</sup> )	$-8.19477 \times 10^{-5} \times T(^{\circ}\text{C}) - 1.92257 \times 10^{-7} \times T2(^{\circ}\text{C}) + 2.5034 \times 10^{-11} \times T3(^{\circ}\text{C}) - 7.2974 \times 10^{-15} \times T4(^{\circ}\text{C}) + 0.137743$
Kinematic Viscosity, (m <sup>2</sup> .s <sup>-1</sup> )	$1 \times 10^{-6} \times \exp((544.149/(T(^{\circ}\text{C})+114.43))-2.59578)$
Dynamic Viscosity, (Pa.s)	$\rho \times 1 \times 10^{-6} \times \exp((544.149/(T(^{\circ}\text{C})+114.43))-2.59578)$

The annulus space between the glass-shield and the HCE is evacuated and is modeled using a very low thermally conducting material as in this region the primary mode of heat transfer is through radiation. In the HCE, the thermic fluid carries away the heat from the metallic pipe through convection, and conduction occurs in the glass-shield and metallic tube wall<sup>[5]</sup>. Table 2 describes the physical properties of the glass shield and metallic pipe. The popular commercial CFD software ANSYS FLUENT allows thin walls to be modeled according to a shell-conduction model<sup>[6]</sup> which does not require the actual solid geometry creation and discretization/meshing<sup>[7]</sup>.

The solar ray has been traced all throughout the day for a representative summer and winter day as being the summer solstice and the winter solstice at the location in Pune, India. The glass-shield allows almost all the solar radiation to pass through it to the HCE. Besides, a 90° sector of the glass tube which faces away from the sun has a heat source from the reflected incident solar radiation coming from the parabolic trough mirror. This highly focused flux is the major contribution of heat to the system and causes very high temperature gradients within the glass-shield.

**Table 2.** Physical properties of material of receiver

<b>Properties</b>	<b>Glass</b>	<b>Steel</b>
Density, (kg.m <sup>-3</sup> )	2220.00	8030.00
Specific heat, (J.kg <sup>-1</sup> .K <sup>-1</sup> )	830.00	502.48
Thermal conductivity, (W.m <sup>-1</sup> . K <sup>-1</sup> )	1.15	16.27

### 3. Governing Equations

The governing equations of fluid flow and heat transfer can be considered as mathematical formulations of the conservation laws of fluid mechanics and are referred to as the Navier-Stokes equations. By enforcing these conservation laws over discrete spatial volumes in a fluid domain, it is possible to achieve a systematic account of the changes in mass, momentum and energy as the flow crosses the volume boundaries<sup>[8]</sup>.

The resulting equations can be written as:

Continuity equation:

$$\frac{\partial \rho}{\partial t} + \frac{\partial}{\partial x_i}(\rho u_i) = 0 \quad (1)$$

Momentum equation:

$$\frac{\partial}{\partial t}(\rho u_i) + \frac{\partial}{\partial x_i}(\rho u_i u_j) = \frac{\partial}{\partial x_j} \left[ -\rho \delta_{ij} + \mu \left( \frac{\partial u_i}{\partial x_j} + \frac{\partial u_j}{\partial x_i} \right) \right] + \rho g_i \quad (2)$$

Energy Equation:

$$\frac{\partial}{\partial t}(\rho C_p T) + \frac{\partial}{\partial x_i}(\rho u_i C_p T) - \frac{\partial}{\partial x_j} \left( \lambda \frac{\partial T}{\partial x_j} \right) = s_T \quad (3)$$

The modeling of the governing involves the solution of some additional transport equations for the turbulence kinetic energy and specific dissipation rate for the Reynolds Average Navier Stokes equation closure by determining the turbulent viscosity. The form used in this analysis is the one proposed by Menter<sup>[11]</sup> for blending the  $k$ - $\omega$  and  $k$ - $\varepsilon$  turbulence models through a blending factor.

Turbulence kinetic energy:

$$\frac{\partial}{\partial t}(\rho k) + \frac{\partial}{\partial x_i}(\rho k u_i) = \frac{\partial}{\partial x_j} \left( \Gamma_k \frac{\partial k}{\partial x_j} \right) + \tilde{G}_k - Y_k + S_k \quad (4)$$

Specific dissipation rate:

$$\frac{\partial}{\partial t}(\rho \omega) + \frac{\partial}{\partial x_i}(\rho \omega u_i) = \frac{\partial}{\partial x_j} \left( \Gamma_\omega \frac{\partial \omega}{\partial x_j} \right) + \tilde{G}_\omega - Y_\omega + D_\omega + S_\omega \quad (5)$$

The right hand side of the above equation consists of diffusion, generation, dissipation and source terms (absent in the present analysis). The specific dissipation rate equation contains an additional term accounting for cross-diffusion effects. All these are model parameters and have their complete description available in published literature<sup>[6]</sup>. The calculation of turbulence kinetic energy and specific dissipation rate are used for evaluating the turbulent viscosity which appears as an additional term in the transport equations.

## 4. Domain description

### a. Geometric modeling

The geometry consists of two concentric cylinders (glass and HCE pipe) with two fluid regions for the thermic fluid (inner cylinder) and the vacuum region (annulus). In the

present analysis, the geometry is considered to be oriented along the z-axis, with positive Z denoting the south direction while the positive X denotes the east direction. Table 3 describes the geometrical parameters of receiver of the PTC.

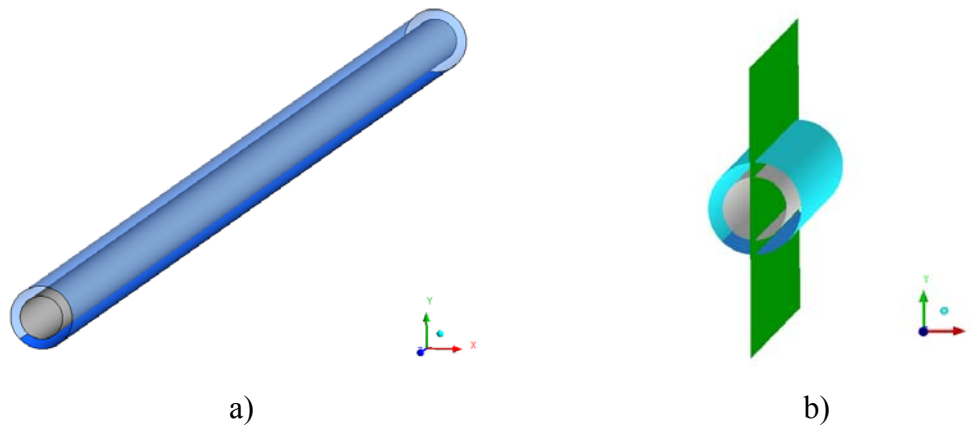


**Fig.2** Modeled initial geometry with bottom sector patch equally across the Y-Z plane

**Table 3.** Geometrical parameters of the PTC's receiver

<b>Receiver configuration</b>	<b>Parameter</b>
Outer diameter of the glass-shield ( <i>m</i> )	0.06
Thickness of the glass-shield ( <i>m</i> )	0.0045
Outer diameter of the HCE ( <i>m</i> )	0.035
Thickness of the HCE ( <i>m</i> )	0.001
Length of the receiver ( <i>m</i> )	1.35

The patch of 90° sector on the outer glass wall is modeled considering it to have a different position for different times of the day in different seasons. This was determined from the solar calculator within the ANSYS FLUENT application<sup>[6]</sup> which helped in locating the exact position of this sector patch. The initial geometry was created and meshed with the patch having the Y-Z plane bisecting through it. Subsequently, the mesh was rotated around the z-axis for the summer and winter conditions based on the calculator inputs for the sun's location. The representative days of summer and winter were considered to be the respective solstice days during which the diurnal conditions were varied for thermal conditions and for mesh orientation while performing ray tracing. The corresponding geometries at three times of the day shown in Fig. 3 depict the relative orientation of the bottom patch (facing away from the Sun), and Table 4 demonstrates the values of transformation angle of rotation for summer and winter.

**Table 4:** Bottom patch's orientation with respect to the the N-S orientation at different time of the day

Time of the day	Transformation angle of rotation with the Y-Z plane (°)	
	Summer	Winter
Early dawn	-76.58	-84.07
Noon	5.44	8.42
Evening	60.07	75.54

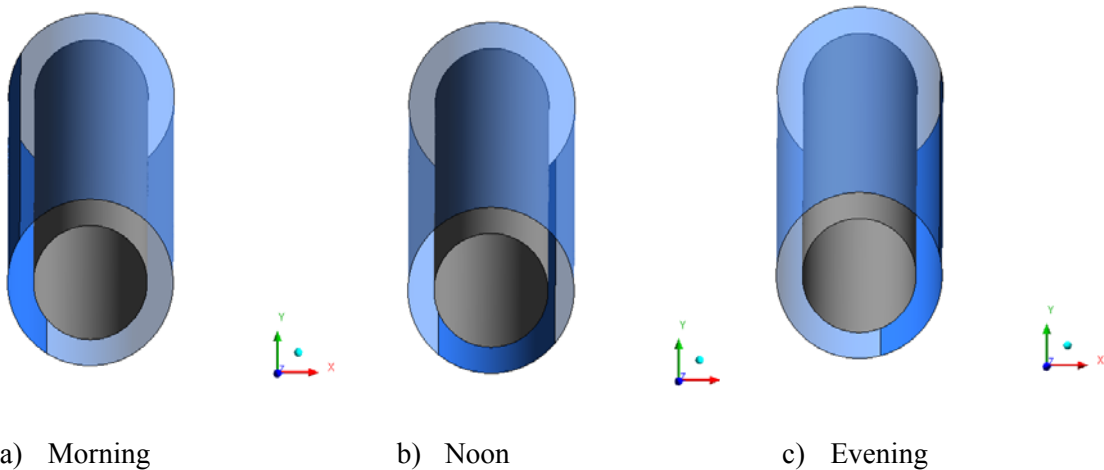


**Fig. 3** Orientation of the sector-patch facing away from the sun and exposed to the reflected beam from the parabolic mirror.

#### *b. Solar Load Model*

ANSYS FLUENT provides a model that can be used to calculate radiation effects from the sun's rays that enter a computational domain. It includes a solar calculator utility that can be used to construct the sun's location in the sky for a given time-of-day, date, and position and can be used to model steady and unsteady flows. It allows simulating solar loading effects and determining the solar transmission through all glazed surfaces over the course of a day. The typical inputs needed are the global position (latitude, longitude and time-zone), starting date and time, grid orientation, solar irradiation method and the sunshine factor. The grid orientation is specified in the North (negative Z axis, in the present case) and East (positive X axis, in the present case) direction vector in the CFD grid with the default solar irradiation method as fair weather conditions. The values computed are the sun direction vector, direct normal solar irradiation at earth's surface, diffuse solar irradiation both for vertical and horizontal surface and ground reflected (diffuse) solar irradiation for vertical surface<sup>[6]</sup>.

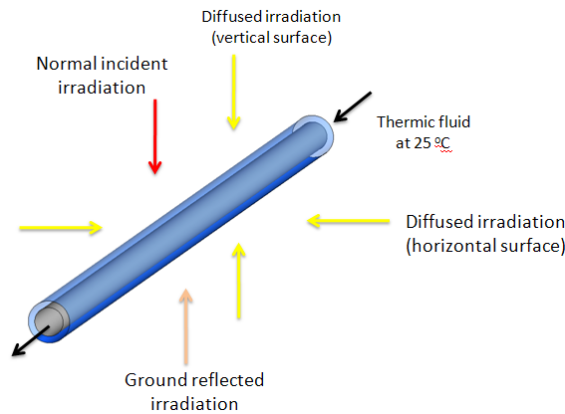
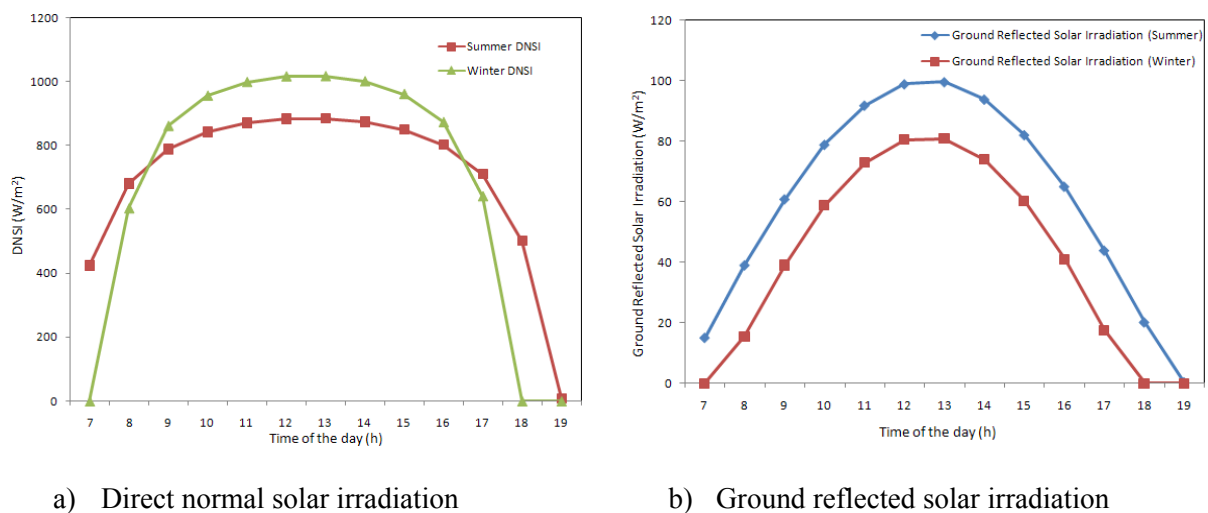


**Fig. 4** Solar irradiative flux distribution

The solar loads calculated by ANSYS FLUENT are based on the published data from ASHRAE Handbook of Fundamentals<sup>[6]</sup>. The direct normal solar irradiation shows a typical bell-shaped curve.



a) Direct normal solar irradiation

b) Ground reflected solar irradiation

**Fig. 5** Diurnal and seasonal variation of direct normal and ground reflected solar irradiation

The summer curve is more uniform while the winter curve has a higher gradient for diurnal variation. The ground reflected solar irradiation (Fig. 5, (b)) on the other hand, shows similar slope for summer and winter conditions although the summer values are higher due to higher incident solar flux on the ground surface. The diffused solar irradiation is different for vertical and horizontal surfaces (Fig. 6). Horizontal diffuse solar flux variations are the typical bell-shaped curves while the vertical surfaces receive a low diffused solar flux at around the noon time as the sun is in overhead position. The curve therefore has two maxima with minima at the noon time of the day.

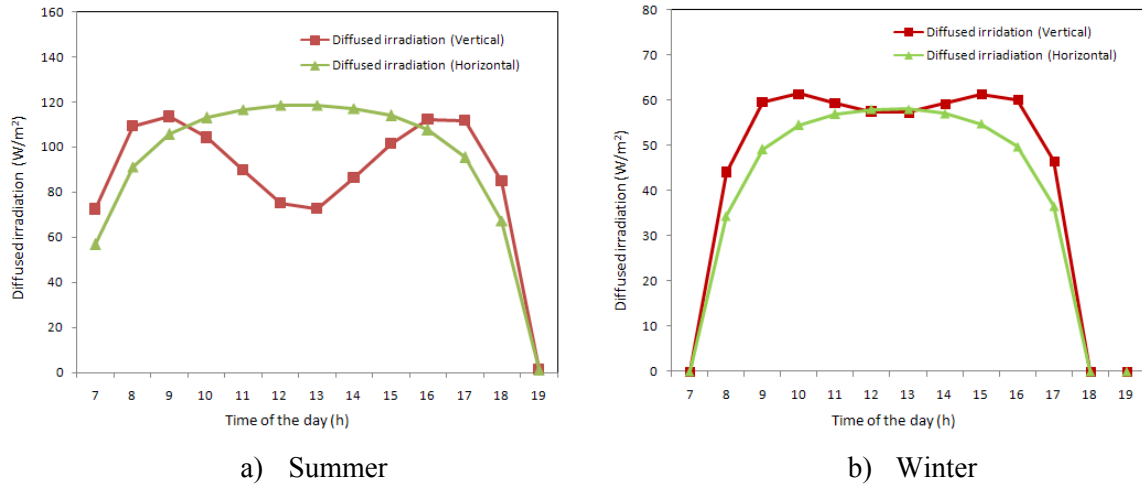


**Fig. 6** Diurnal and seasonal variation of diffuse solar irradiation

*c. Radiation Model*

The surface-to-surface radiation model makes it possible to simulate thermal radiation exchange between diffuse surfaces forming a closed set. The medium that fills the space between the surfaces is non-participating, i.e., it does not absorb, emit, or scatter any radiation. Therefore, the amount of radiation received and emitted by each surface is uniquely defined by the surface's optical properties and the thermal boundary conditions imposed on it.

*d. Standard  $k-\omega$  SST model with low- $Re$  corrections*

The SST  $k-\omega$  turbulence model is a popular two-equation eddy-viscosity model in which the shear stress transport (SST) formulation combines the best of two worlds. The use of a  $k-\omega$  formulation in the inner parts of the boundary layer makes the model directly usable all the way down to the wall through the viscous sub-layer. Hence the SST  $k-\omega$  model can be used as a low- $Re$  turbulence model without any extra damping functions. The SST formulation also switches to a standard  $k-\varepsilon$  behavior in the free-stream and thereby avoids the common  $k-\omega$  problem that the model is too sensitive to the inlet free-stream turbulence properties. The model shows good behavior in adverse pressure gradients and separating flow although it does produce a bit too large turbulence levels in regions with large normal strain, but is much less pronounced than with a normal  $k-\varepsilon$  model.

**5. Boundary conditions**

a. *Flow conditions:* The flow at the inlet was maintained as uniform mass flow at ambient temperature conditions. A low  $Re$  is typical for HCE applications for Parabolic

Trough Collectors which ranged from 1000 to around 8000 in the domain. This variation is due to highly temperature dependent viscosity. The vacuum region is modelled by assuming it to be a fluid with very high viscosity and the velocity components have been fixed at zero values a typical approach followed among CFD practitioners. The outlet is maintained to be at ambient pressure. The reverse flow direction was calculated by the in-built feature in ANSYS FLUENT for calculating it from the neighbouring cells. The walls are said to have no-slip boundary conditions. Due to the highly asymmetric nature of the physics and geometry, the full three dimensional domain has been considered for analysis with no symmetric boundaries.

b. *Thermal conditions:* The thermic fluid entering under ambient conditions is considered to undergo a thermally developing flow due to the concentration of heat from the parabolic mirror. Due to reverse flow being encountered at the outlet, the backflow temperature was implemented using an interpreted User-Defined Function (UDF) which assigned the mass-weighted average temperature at the outlet. The UDF also accounted for the temperature dependent viscosity which was of an exponential form. The polynomial function available from the Therminol-VP1™ properties [4] were implemented in FLUENT as polynomial specification after appropriate transformation of temperature functions to Kelvin scale. This was done using the *horner()* function available with the open source software SCILAB. As described above, the solar load model takes care of the appropriate heat fluxes on the domain also taking into account, the shadowing effect due to semi-transparent surfaces (glass) and opaque surfaces (HCE).

The receiver having a 90° sector patch facing the parabolic mirror is given a heat source flux, which is concentrated from the mirror onto the focal line, where the receiver is placed. The value of flux has been calculated from the normal solar irradiation incident on the mirror of around 3 m<sup>2</sup> of aperture area, with appropriate efficiency for mirror's reflectivity (0.9) and intercept factor (0.9) of the receiver. The outer glass-shield was assumed to be exposed to ambient temperature with a constant convection heat transfer coefficient for modeling outside wind conditions.

**Table 5.** DNSI for flux calculations for the bottom glass surface (90° sector)

Time of the day	Normal Direct Irradiation (W/m <sup>2</sup> )	
	<i>Summer</i>	<i>Winter</i>
Early dawn	423.97	264.44
Noon	884.82	1017.06
Evening	711.08	641.54

c. *Radiation boundary conditions*

The S2S radiation model requires the calculation of the view-factors which has been done using the ray-tracing method. As the surface to surface radiation is prominent in the vacuum region, the participating zones considered are only the glass-shield and outer surface of the HCE tube. The solar ray tracing algorithm requires the description of the surfaces involved in the ray-tracing to be defined as either semi-transparent or opaque for accurate shadowing effect calculations. In the present analysis, the HCE metallic tube is considered as an opaque surface while the outer glass-shield has been considered to be semi-transparent with optical properties as tabulated below.

**Table 6.** Optical properties of glass

	<b>Spectrum type</b>	<b>Incident</b>	<b>Diffused</b>
<b>Absorbance, (<math>\alpha</math>)</b>	Visible	0.09	0.1
	Infrared	0.09	
<b>Transmittance, (<math>\tau</math>)</b>	Visible	0.83	0.75
	Infrared	0.83	
<b>Reflectance, (<math>r</math>)</b>	Visible	0.08	0.84
	Infrared	0.08	

## 6. Numerical methodology

The geometry was discretized with a structured multi-block mesh generated using the GAMBIT through geometry decomposition, Fig. 7. The complete geometry was divided into around half-a-million cells for performing the coupled flow and thermal analysis.

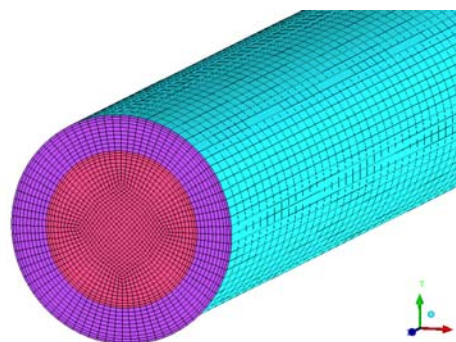


**Fig. 7** Structured Multi-block mesh

The governing equations were solved using the finite volume method by the pressure-based segregated spatially implicit solver available with ANSYS FLUENT 12.1. The 3-D steady state conservations equations are thereby, solved independently with the coupling

between the momentum and the continuity equations being achieved using the pressure-correction equation approach Semi-Implicit Method for Pressure Linked Equations, as proposed by Spalding and Patankar<sup>[10]</sup>. The first order upwind differencing scheme is implemented for the momentum and energy equations. The PRESTO! scheme for pressure interpolation has been used since it is appropriate for density variations and swirling flows under gravitational field.

The convergence was monitored keeping the residual target for all equations as  $10^{-4}$  except for the energy equation, for which a target of  $10^{-7}$  was used, Fig. 8. This was achieved in most of the cases that were considered for the present analysis. Additional monitor of average outlet temperature was also analyzed to ensuring appropriate convergence. The convergence difficulties were usually because of the vacuum modeling performed using a pseudo-fluid whose velocity components were fixed at zero value while radiation effects were modeled using S2S model.

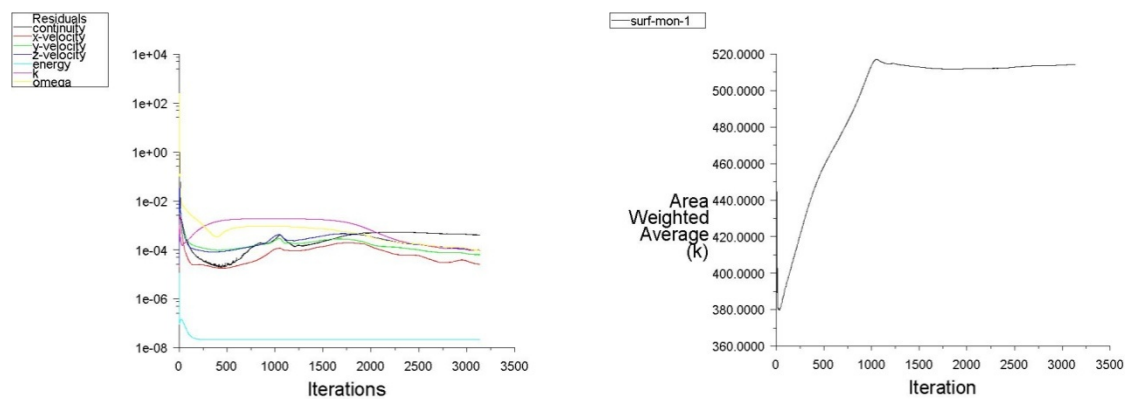


**Fig. 8** Convergence history for a typical simulation

A typical solution required around 3500 iterations to converge and this meant a simulation time of around 30 hours on a 1.60 GHz Intel micro-processor with 2 GB RAM. All simulations were performed with ANSYS FLUENT module considered in a stand-alone mode. The input parameters were defined for different cases and the corresponding output parameters were obtained with the parameterization feature available with ANSYS FLUENT.

## 7. Results and Discussion

The analyses of the simulations were done using the key features of ANSYS FLUENT and ANSYS CFD Post for efficient and good quality post-processing. The



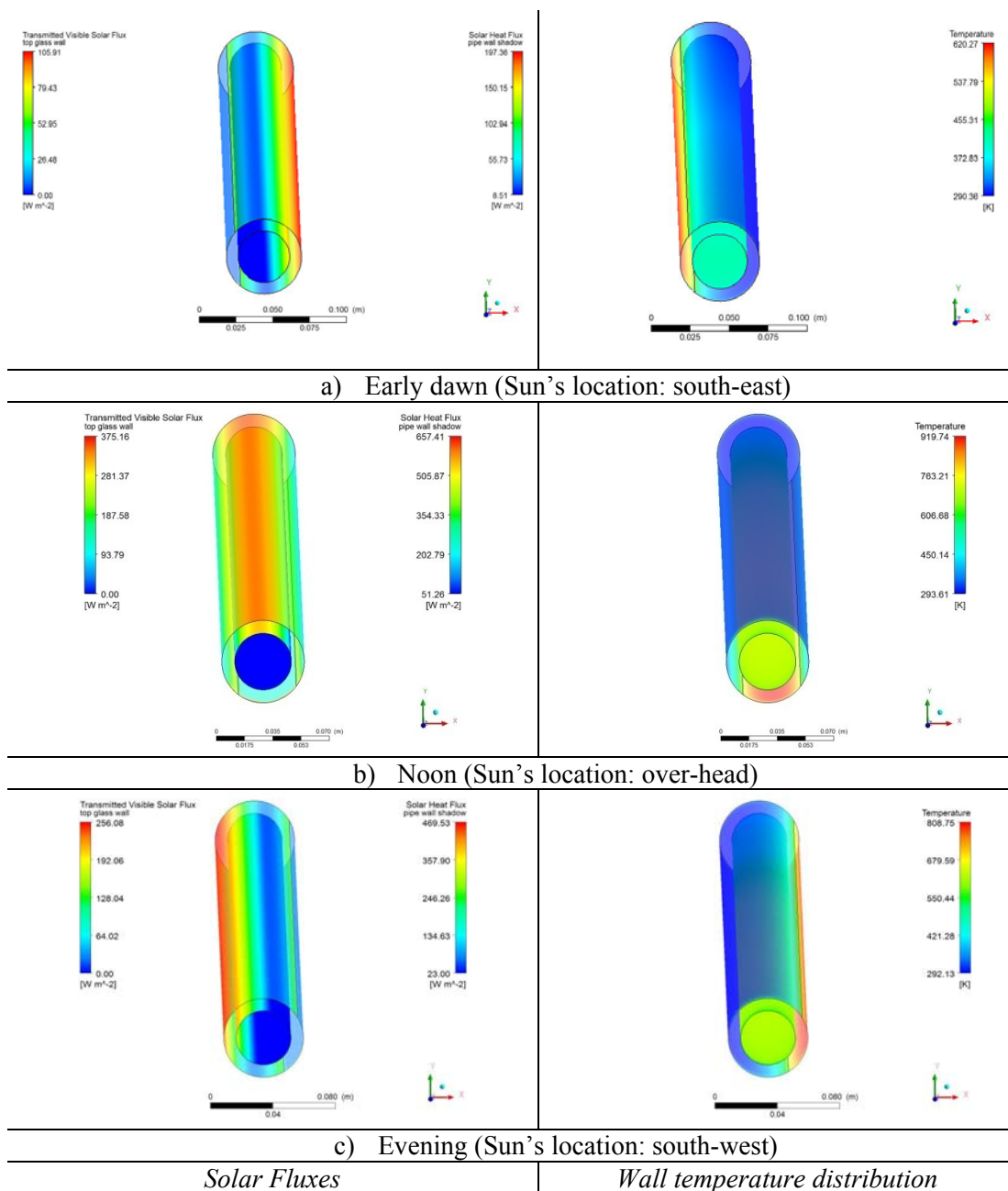


**Fig. 10** Thermal analysis during winter conditions

As described earlier, the PTC is modeled to follow the Sun's position while being placed along the N-S orientation. This meant that the bottom surface of the glass shield is always in the shadow of the HCE tube carrying the thermic fluid. Due to the higher transmittance of glass, the top surface of the glass shield ensures that the HCE pipe receives maximum heat flux. The contours plotted on the HCE inside the glass-shield are a hybrid type, with transmitted visible solar flux plotted on the outer glass-shield while the inner HCE pipe is colored by solar heat flux (incident, diffused and ground reflected). Such hybrid plots

are possible using ANSYS CFD Post and is very useful for analyzing the combined effect of two different phenomena on the same plot as has been done in the present case.

All the transmitted heat flux plots confirm that the shadowing effects are well taken into account. This effect is visible all the more by the contours of Solar Heat flux on the pipe-wall which shows a minimum on the side facing away from the sun, the only flux being due to diffused radiation and ground reflected solar irradiation. The plots reveal interesting facts about the summer and winter conditions. While the summer conditions offer a more sustained solar heat and increase the temperature of the wall surfaces to very high values, the solar heat flux during winter noon is marginally higher than the summer noon. The temperature on the bottom glass surface rises to over 800 °C on summer noon as it is exposed to high values of reflected solar radiation from the parabolic trough. This requires a very good quality of glass to be used for such application to avoid damage to the overall set-up. Such facts are well realized using this CFD approach which would otherwise be not easy to visualize. The plots under winter conditions reveal a sharp peak in the incident solar flux while the temperatures rise to a maximum under the noon-day sun. The overall temperature values in the winter conditions are much lower on the HCE inside the glass-shield.

### 7.2 Temperature variation

Fig. 11 shows the plot of temperature variation of Therminol VP1 along the length (at centre-line) of the HCE for summer and winter season at three times of the day i.e. morning, noon and evening. It can be seen that the temperature rise at noon for a day in summer is about 457°C, while for winter is about 390°C. These findings are in accordance with the expected results due to the cold conditions in winter.

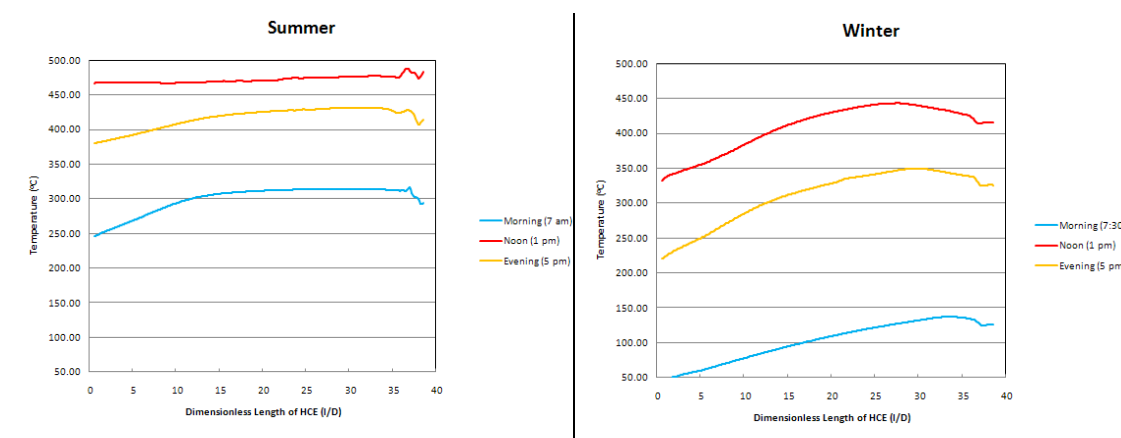


**Fig. 11** Variation of temperature along the length of the HCE

**Table 7.** Temperature rise in the HCE

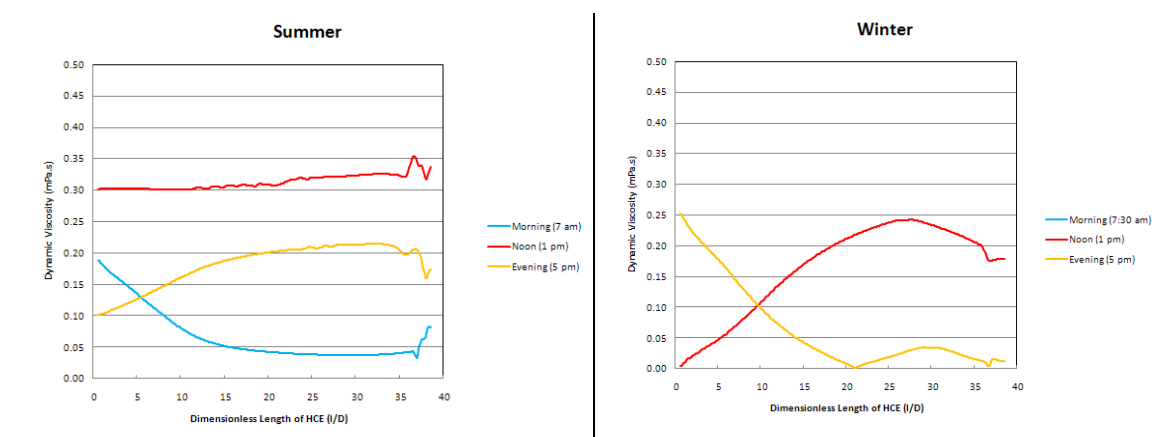
<b>Time of the day</b>	<b>Summer (<math>\Delta T</math>, °C)</b>	<b>Winter (<math>\Delta T</math>, °C)</b>
Early Dawn	268.83	100.66
Noon	<b>457.73</b>	390.61
Evening	388.75	300.71

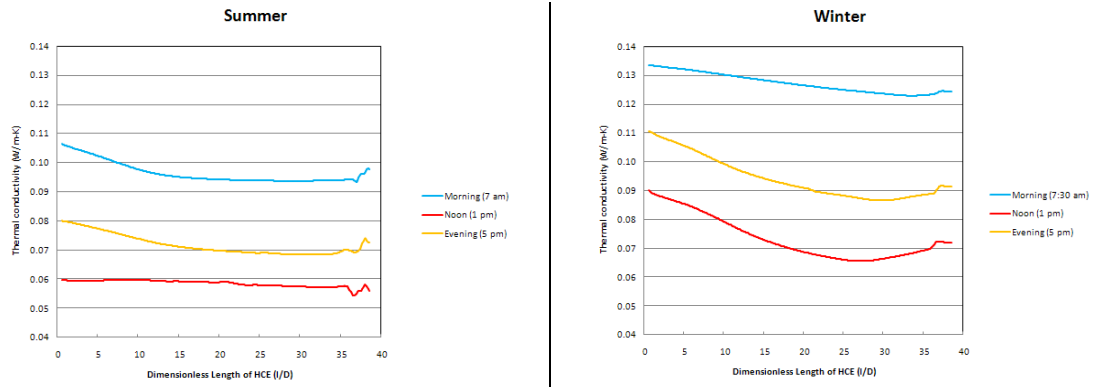
**Table 8.** Maximum temperature inside the HCE

<b>Time of the day</b>	<b>Summer (<math>T_{max}</math>, °C)</b>	<b>Winter (<math>T_{max}</math>, °C)</b>
Early Dawn	356.89	139.40
Noon	<b>657.28</b>	445.67
Evening	504.48	352.00

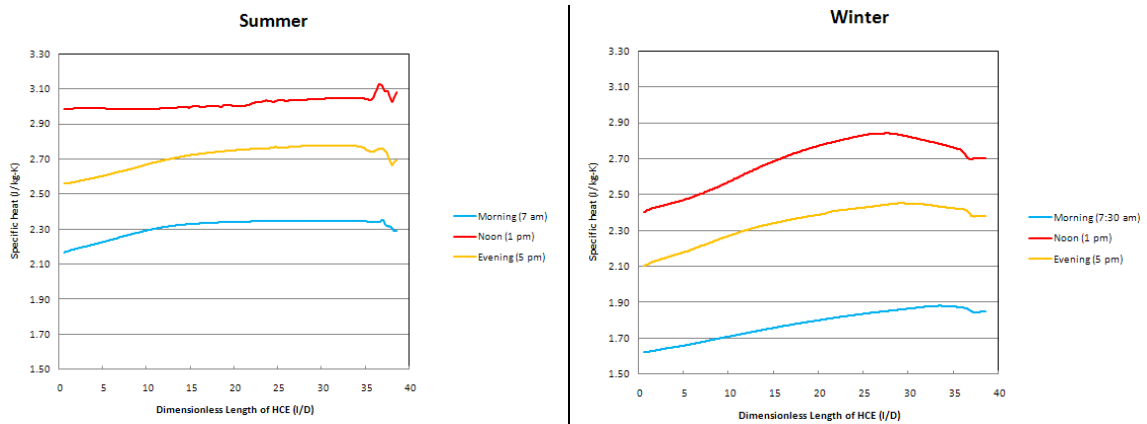
### 7.3 Property variation of the thermic fluid in HCE

Fig. 12-15 describe the variation of the properties for Therminol VP1, namely, dynamic viscosity ( $\mu$ , mPa.s) thermal conductivity ( $k$ ,  $\text{Wm}^{-1}\text{K}^{-1}$ ), specific heat ( $C_p$ ,  $\text{J kg}^{-1}\text{K}^{-1}$ ) and Prandtl number ( $Pr$ ) along the length (at centre-line) of the HCE for a day in summer and winter. It can be seen that as expected from the plot of  $Pr$ , the dynamic viscosity and specific heat, respectively, at noon timing of the day are in the range of 0.32 mPa.s and  $3 \text{ W kg}^{-1}\text{K}^{-1}$  in summer and less than 0.25mPa.s and  $2.6 \text{ W kg}^{-1}\text{K}^{-1}$  in winter. Also the values of thermal conductivity for the same time are about  $0.06 \text{ Wm}^{-1}\text{K}^{-1}$  in summer whereas it decreases from 0.09 to  $0.065 \text{ Wm}^{-1}\text{K}^{-1}$ . This also concludes that as the temperature of the receiver in summer is high these properties do not show a greater change as compared to those in winter when the conditions are a bit cold both in morning and evening so the fluid warms up initially before attaining a constant value.

**Fig. 12** Variation of dynamic viscosity along the length of the HCE



**Fig. 13** Variation of thermal conductivity along the length of the HCE



**Fig. 14** Variation of specific heat along the length of the HCE

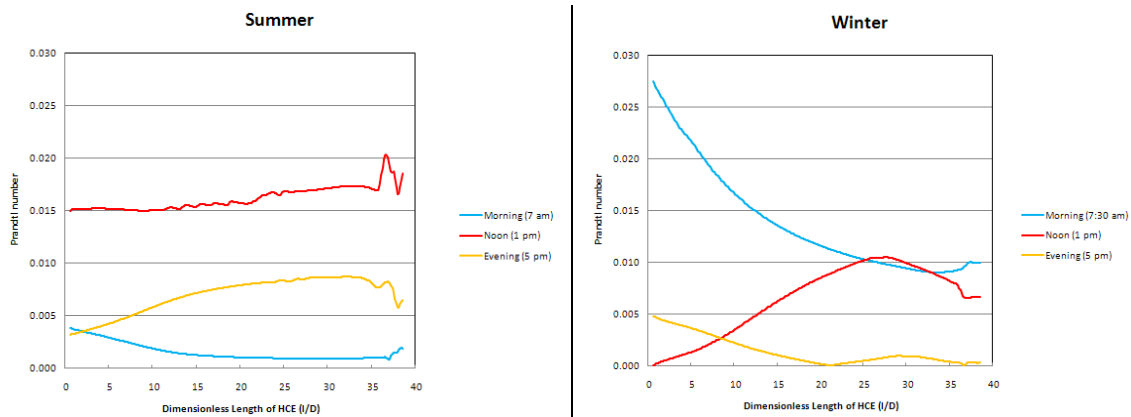


**Fig. 15** Variation of Prandtl number along the length of the HCE

#### 7.4 Flow behavior

The flow phenomenon displays a highly three dimensional swirling pattern especially due to the asymmetric heating of the HCE tube transferring energy to the thermic fluid with highly temperature dependent properties.

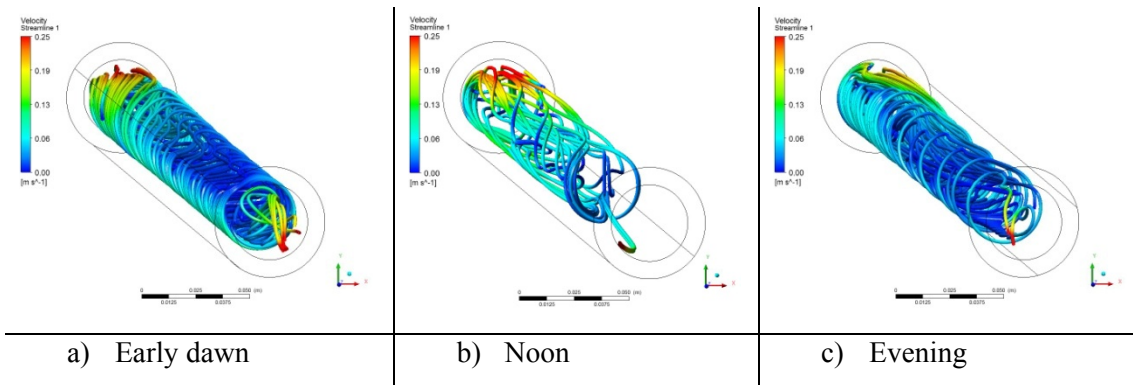
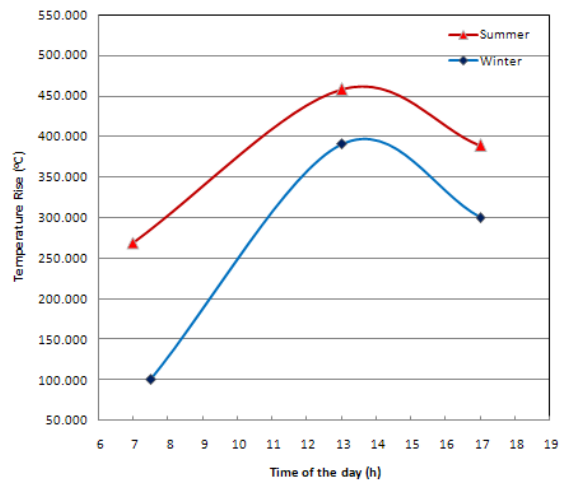
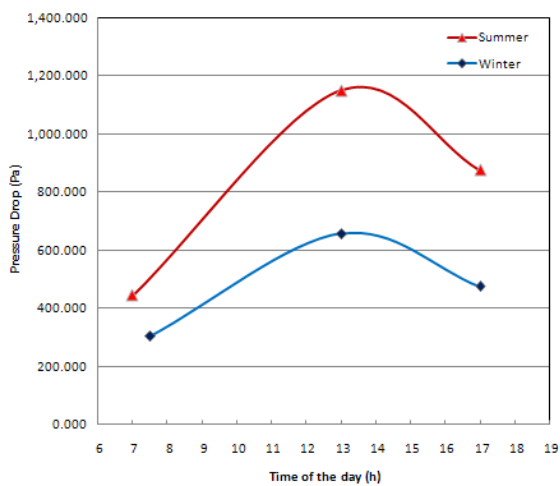


**Fig. 16** Flow streamlines under steady flow showing the highly swirling phenomenon

The highly turbulent eddies ensure a high residence time of the fluid inside the HCE element thereby allowing it efficiently absorb heat and transfer it across the HCE tube. The load on the pump maintaining a constant mass flow rate thereby increase but can be justified by the high amount of thermal energy that the thermic fluid carries. A typical observation was that under noon conditions, the turbulence created in the tube is not as significant as compared to the morning and evening conditions. This is primarily because the parabolic trough mirror focuses the heat on the HCE asymmetrically from the sides compared to the noon conditions when the mirror is right below the HCE tube. The density being a function of temperature causes enhanced turbulence under the downward gravity.



a) Pressure drop

b) Temperature rise

**Fig. 17** Pressure drop and temperature rise of the thermic fluid across the HCE

Nevertheless, the pressure drop of the thermic fluid flow across the HCE is much higher during the noon time compared to the morning and evening conditions. This diurnal trend is observed both for summer as well as winter conditions although the winter values exhibit only vary marginally. This may be attributed to the higher temperatures during the

summer time compared to the winter conditions. As discussed earlier, the winter temperatures variations are much more significant compared to the summer trends.

## **8. Conclusion**

This study analyzed the 3-D conjugate heat transfer mechanism involved in the receiver element of a Parabolic Trough Solar Collector. The in-built Solar Load Model has been used for ray-tracing whose shadowing effects have been verified by the incident and absorbed solar heat flux plots on the glass-shield and HCE, respectively. The thermic fluid flow calculations have been performed by numerically solving the continuity, momentum and energy equations with temperature dependent fluid properties and the turbulence closure has been done using the RANS based  $k-\omega$  SST turbulence model with low-Re corrections. The temperature variation along the flow direction of the thermic fluid shows a case-specific length for attaining fully developed thermal conditions which is much shorter during the summer days compared to those in winter. The natural convection effects influence the flow pattern especially in the morning and evening conditions due to sideways heating from the reflected radiation from the parabolic mirror as is evident in the flow streamlines. This increases the turbulent structures which in-turn increase the residence time of the thermic fluid within the HCE ensuring enhanced heat transfer from the HCE. The diurnal variation of the pressure drop exhibit a two times higher slope under summer conditions compared to that in winter. The temperature rise at noon time is nevertheless very high due to the large solar fluxes. The winter conditions exhibit a comparatively steeper variation for the temperature rise diurnally.

## **Acknowledgements**

The authors would like to acknowledge the contribution of our colleagues Rakesh Belpande and Praful Dandagaval for their assistance with meshing and theoretical inputs.

## Nomenclature

$I$	Irradiance ( $\text{W m}^{-2}$ )
$Pr$	Prandtl number
$Re$	Reynolds number
$T$	temperature ( $^{\circ}\text{C}$ )
$u, v, w$	$x, y, z$ velocity components ( $\text{ms}^{-1}$ )
$x, y, z$	Cartesian coordinates
$g_i$	Directional gravitational acceleration
$k$	Turbulence kinetic energy
$\omega$	Specific dissipation rate for turbulence kinetic energy
$\tilde{G}_q$	Production term in the turbulence equation for the quantity $q$ $\{q = k, \omega\}$
$Y_q$	Dissipation term in the turbulence transport equation for the quantity $q$ $\{q = k, \omega\}$
$D_\omega$	Cross diffusion term for the specific dissipation rate of turbulence kinetic energy
$S_q$	Source term in the turbulence equation for the quantity $q$ $\{q = k, \omega\}$
$C_p$	Specific heat ( $\text{J kg}^{-1} \text{K}^{-1}$ )
$s_T$	Energy source term
$\alpha$	Absorptance
$\tau$	Transmittance
$r$	Reflectance
$\mu$	dynamic viscosity ( $\text{Pa s}$ )
$\lambda$	thermal conductivity
$\rho$	density ( $\text{kg.m}^{-3}$ )
$\Delta$	delta

## References

1. Fernandez-Garcia, E. Zarza, L. Valenzuela, M. Perez. (2010) Parabolic-trough solar collectors and their applications. *Renewable and Sustainable Energy Reviews* 14, pp. 1695-1721.
2. H. Price, E. Lüpfert, D. Kearney, E. Zarza. (2002) Advances in parabolic trough solar power technology. *J. Sol. Energy Eng.* 124, pp 109–125.
3. S.A. Kalogirou. (2004) Solar thermal collectors and applications, *Prog. Energy Combustion Sci.* 30, pp 231–295.
4. M.J. Montes, A. Abanades, J.M. Martinez-Val, M. Valdes. (2009) Solar multiple optimization for a solar-only thermal power plant, using oil as heat transfer fluid in the parabolic trough collectors. *Solar Energy* 83, pp 2165-2176.
5. Reddy KS, Ravi Kumar K, Satyanarayana GV. (2008) Numerical investigation of energy efficient receiver for solar parabolic trough concentrator. *Journal of Heat Transfer Engg.*, 29, pp 961–72.
6. ANSYS Inc., ANSYS Fluent 12.1, User's Guide, 2009.
7. Kalogirou S., Lloyd S. and Ward J. (1997) Modelling, optimization and performance evaluation of a parabolic solar collector steam generation system. *Solar Energy*, 60, 49–59.
8. Z.D. Cheng, Y.L. He, J. Xiao, Y.B. Tao, R.J. Xu. (2010) Three-dimensional numerical study of heat transfer characteristics in the receiver tube of parabolic trough solar collector. *International Communications in Heat and Mass Transfer*. 37 (2010) 782–787.
9. ASHRAE (2001) *Handbook of Fundamentals*. Vol 1, Chapter 30.
10. D.B. Spalding and S.V. Patankar (1980). *Numerical Heat Transfer and Fluid Flow*. Taylor & Francis. ISBN 978-0891165224.
11. F. R. Menter. (1994) Two-Equation Eddy-Viscosity Turbulence Models for Engineering Applications. *AIAA Journal*, 32(8):1598-1605.